Chinese Journal of Mechanical Engineering

ORIGINAL ARTICLE

Open Access

Application of Nonlinear Lamb Wave Mixing Method for Residual Stress Measurement in Metal Plate

Jingpin Jiao*, Li Li, Xiang Gao, Quan Cheng, Cunfu He and Bin Wu

Abstract

Harmonic nonlinear ultrasound can offer high sensitivity for residual stress measurements; however, it cannot be used for local stress measurements at a point in space and exhibits nonlinear distortions in the experimental system. This paper presents a feasibility study on the measurement of residual stress in a metal plate using a nonlinear Lamb wave-mixing technique. The resonant conditions for two Lamb waves to generate a mixing frequency wave are obtained via theoretical analysis. Finite element simulations are performed to investigate the nonlinear interactions between the two Lamb waves. Results show that two incident A0 waves interact in regions of material nonlinearity and generate a rightward S0 wave at the sum frequency. Residual stress measurement experiments are conducted on steel plate specimens using the collinear Lamb wave-mixing technique. By setting different delays for two transmitters, the generated sum-frequency component at different spatial locations is measured. Experimental results show that the spatial distribution of the amplitude of the sum-frequency component agrees well with the spatial distribution of the residual stress measured using X-rays. The proposed collinear Lamb wave-mixing method is effective for measuring the distribution of residual stress in metal plates.

Keywords Residual stress, Lamb wave, Collinear wave mixing, Nondestructive testing, Resonant conditions

1 Introduction

Residual stress is the internal stress within a structure that remains stationary and maintains equilibrium with its surroundings [1]. Residual stress is generated owing to nonuniform elastoplastic deformation after external forces or inhomogeneous temperature fields are removed. Residual stresses significantly affect the properties of mechanical components, such as their deformation, fatigue strength, dimensional stability, corrosion resistance, and brittleness, thereby affecting their performance [2, 3]. Many engineering accidents and disasters are associated with residual stress; therefore, residual stress measurements are critical for structural performance assessment and failure prevention [4].

Residual stress measurement techniques can be classified into two categories: destructive and nondestructive methods [5, 6]. Destructive methods, such as hole drilling, slicing, or ring coring, facilitate stress release but can cause irreversible damage to the material [7, 8]. Recently, nondestructive testing methods, such as X-ray diffraction, digital image correlation, magnetic methods, and ultrasonic methods, have been used widely for detecting residual stress [9, 10]. X-ray diffraction can estimate the residual stress on surface of components by measuring the lattice spacing of materials; however, its sensitivity is significantly affected by surface conditions [11]. Digital image correlation allows noncontact estimation of the stress field by calculating the correlation of images obtained under stress-free and stressed conditions [12]. However, this technique requires a speckle

*Correspondence:
Jingpin Jiao
jiaojp@bjut.edu.cn
Faculty of Materials and Manufacturing, Beijing University of Technology, Beijing 100124, China

pattern on the surface of the target structure and is not suitable for continuous monitoring. Magnetic methods, such as Barkhausen [13], can estimate the residual stress of materials based on the relationship between the stress and magnetization curve during ferromagnetic saturation; however, they are only applicable to ferromagnetic materials.

Ultrasonic testing is a more convenient and efficient technique for residual-stress measurement compared with other non-destructive testing (NDT) methods. Stress measurement based on ultrasonic waves primarily involves the acousto-elastic effect, wherein the velocity of the ultrasonic wave is linearly related to the stress of the material as it propagates through the material [14–16]. Studies pertaining to stress measurements using the acousto-elastic effect involves multiple modes of ultrasonic waves, such as conventional bulk, guided, Rayleigh, Lamb, and longitudinal critically refracted waves [17–20]. In particular, the longitudinal critically refracted wave is widely adopted for stress measurement because of its sensitivity to inherent stress, as it propagates beneath the surface to a depth equivalent to the wavelength. In most materials, the variation in wave velocity caused by internal stress is insignificant; therefore, the acoustoelastic effect is extremely weak [21]. For example, a stress variation of 100 MPa can only change the wave velocity in steel by 0.01% [22]. Consequently, residual stress measurement methods based on the acoustoelastic effect exhibit low sensitivity and require high accuracy for measuring the arrival time of the ultrasonic wave packet.

Compared with conventional linear ultrasonic technologies, nonlinear ultrasonic testing technology is more sensitive to microstructural changes in a material [23–25]. Studies indicate that the stress of mechanical components can affect the nonlinear properties of ultrasonic waves [26, 27]. Stress-induced microstructural evolution of mechanical components can result in ultrasonic distortion, and higher harmonics associated with stress are generated. In addition, the theoretical relationship between the nonlinear coefficients and stress can be represented by a dislocation model. Nonlinear ultrasonic testing has been successfully performed to assess residual stress in mechanical components. Experiments were conducted to confirm the relationship between the amplitude of the second harmonics and residual stress [28]. For example, Yan et al. [29] experimentally investigated the variation of the surface wave nonlinear coefficient with increasing tensile stress; Liu et al. [30] experimentally investigated the propagation of nonlinear surface waves in aluminum alloy (AA 7075) samples shot-peened at different peening intensities and demonstrated the feasibility of nonlinear surface waves for residual stress measurements; Mao et al. [31] applied nonlinear critically refracted longitudinal waves to evaluate the stress state of metallic materials under steady state. The experimental results showed that the second- and third-order relative nonlinear coefficients increased monotonically with stress, and that the normalized relationship was consistent with the simplified dislocation model.

Although the aforementioned nonlinear ultrasonic methods based on the effects of harmonic generation can offer higher sensitivity for residual-stress measurements [32], these methods cannot be used for local-stress measurements at a point in space. The nonlinear coefficients measured by these methods are the cumulative nonlinear responses in the region between the transmitter and receiver; therefore, the measured stresses are also the average stresses in the corresponding region.

This limitation can be overcome using the wave-mixing technique, which is based on the fact that the nonlinear interaction of two incident waves with nonlinear sources (such as material nonlinearity or micro-damage) can generate a third wave (known as the mixing frequency wave), whose frequency and wave vector are the sum of the incident frequencies and wave vectors, respectively [23, 24, 32]. Notably, the measured nonlinearity is related only to the acoustic nonlinearity within the mixing zone [33]. Thus, the spatial distribution of the nonlinear sources in the structure can be obtained by adjusting the intersection positions of the two incident waves.

The main objective of this study is to conduct a feasibility study on the measurement of residual stress in metal plates using a nonlinear Lamb wave mixing technique. First, a theoretical analysis was performed to determine the resonant conditions for generating the mixing frequency effect of two Lamb waves. Subsequently, finite element simulations were performed to investigate the nonlinear interaction of the two Lamb waves in regions of material nonlinearity. Finally, residual stress measurement experiments were performed on the steel plate specimens using the collinear Lamb wave mixing technique.

2 Fundamental Theories of Nonlinear Analysis

Under certain resonant conditions, two incident waves (ω_1 and ω_2) interact with the nonlinear source to generate a mixing frequency wave (ω_g). The resonant conditions for its generation are as follows:

$$\begin{cases} \omega_g = \omega_1 \pm \omega_2, \\ \boldsymbol{k}_g = \boldsymbol{k}_1 \pm \boldsymbol{k}_2, \end{cases} \tag{1}$$

where $\boldsymbol{k}_1$, $\boldsymbol{k}_2$, and $\boldsymbol{k}_g$ are the wave vectors of two incident waves and the mixing frequency wave, respectively; "+"

indicates sum frequency; "−" indicates the difference frequency.

Furthermore, the relationship between the two incident waves and mixing frequency waves can be represented by the geometry shown in Figure 1, where α is the interaction angle of the two incident waves, and ψ is the scattering angle.

For Lamb wave mixing, in addition to the aforementioned resonance conditions, the dispersion relationship of the Lamb wave must be satisfied.

Considering the dispersion characteristics of Lamb waves, the resonance conditions for two incident Lamb waves for generating the mixing frequency waves can be expressed as follows:

$$\begin{cases} (K_{\text{sum}})^2 = (K_1)^2 + (K_2)^2 + 2K_1K_2\cos\alpha, \\ (K_2)^2 = (K_1)^2 + (K_{\text{sum}})^2 - 2K_1K_{\text{sum}}\cos\psi, \end{cases} \tag{2}$$

$$\begin{cases} (K_{\text{dif}})^2 = (K_1)^2 + (K_2)^2 - 2K_1K_2\cos\alpha, \\ (K_2)^2 = (K_1)^2 + (K_{\text{dif}})^2 - 2K_1K_{\text{dif}}\cos\psi, \end{cases} \tag{3}$$

where, K_1 and K_2 are the wave numbers of two incident waves, whereas K_{sum} and K_{dif} are the wave numbers of the sum-frequency and difference-frequency waves, respectively. The wave numbers in the expressions above can be expressed by the dispersion characteristics of Lamb waves.

$$\begin{cases} K_1 = \dfrac{2\pi f_1}{v_{p(f_1)}}, \quad K_2 = \dfrac{2\pi f_2}{v_{p(f_2)}}, \\ K_{\text{sum}} = \dfrac{2\pi(f_1+f_2)}{v_{p(f_1+f_2)}}, \ K_{\text{dif}} = \dfrac{2\pi(f_1-f_2)}{v_{p(f_1-f_2)}}, \end{cases} \tag{4}$$

where $v_{p(f1)}$ and $v_{p(f2)}$ are the phase velocities of two incident Lamb waves; $v_{p(f1+f2)}$ and $v_{p(f1\text{-}f2)}$ are the phase velocities of the sum-frequency and difference-frequency waves, respectively.

Furthermore, the interaction angle α and scattering angle ψ for sum-frequency and difference-frequency Lamb waves can be expressed as follows:

$$\begin{cases} \cos\alpha = \dfrac{v_{p(f_1)}}{2f_1}\dfrac{v_{p(f_2)}}{f_2}\left\{\left(\dfrac{f_1+f_2}{v_{p(f_1+f_2)}}\right)^2 - \left(\dfrac{f_1}{v_{p(f_1)}}\right)^2 - \left(\dfrac{f_2}{v_{p(f_2)}}\right)^2\right\}, \\ \cos\psi = \dfrac{v_{p(f_1)}}{2f_1}\dfrac{v_{p(f_1+f_2)}}{f_1+f_2}\left\{\left(\dfrac{f_1}{v_{p(f_1)}}\right)^2 + \left(\dfrac{f_1+f_2}{v_{p(f_1+f_2)}}\right)^2 - \left(\dfrac{f_2}{v_{p(f_2)}}\right)^2\right\}, \end{cases} \tag{5}$$

$$\begin{cases} \cos\alpha = \dfrac{v_{p(f_1)}}{2f_1}\dfrac{v_{p(f_2)}}{f_2}\left\{\left(\dfrac{f_1}{v_{p(f_1)}}\right)^2 + \left(\dfrac{f_2}{v_{p(f_2)}}\right)^2 - \left(\dfrac{f_1-f_2}{v_{p(f_1-f_2)}}\right)^2\right\}, \\ \cos\psi = \dfrac{v_{p(f_1)}}{2f_1}\dfrac{v_{p(f_2)}}{f_1-f_2}\left\{\left(\dfrac{f_1}{v_{p(f_1)}}\right)^2 + \left(\dfrac{f_1-f_2}{v_{p(f_1-f_2)}}\right)^2 - \left(\dfrac{f_2}{v_{p(f_2)}}\right)^2\right\}, \end{cases} \tag{6}$$

As shown in Eqs. (5) and (6), the incident angle and scattering angle are related to the frequencies and phase velocities of the incident and mixing frequency waves. As an example, Figure 2 shows the resonant conditions for the interaction of two A0 waves resulting in the generation of a sum-frequency S_0 wave in an aluminum plate with a thickness of 1 mm when the incident excitation frequency $f_1 = 1.26$ MHz.

When the incident frequency f_2 is 0.32 MHz and incident angle is 180°, the two incident A0 waves will interact, resulting in the generation of a sum-frequency S0 wave. Moreover, the scattering angle is 0°, which implies

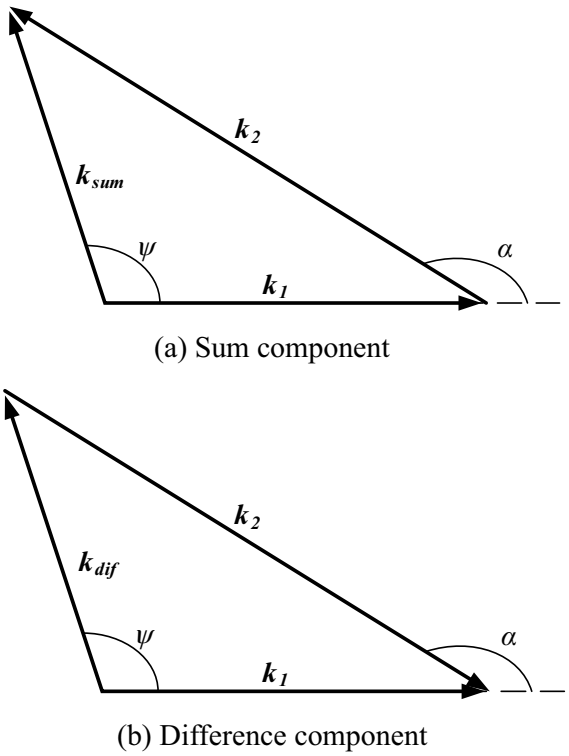

Figure 1 Geometric representation of two incident waves and generated mixing frequency wave

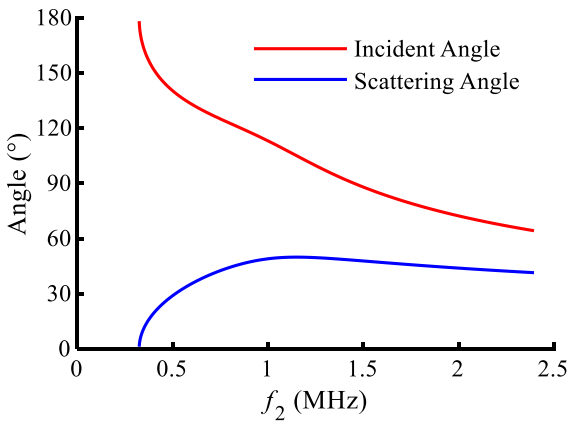

Figure 2 Resonant conditions in aluminum plate for interaction of two A0 waves to generate S0 wave

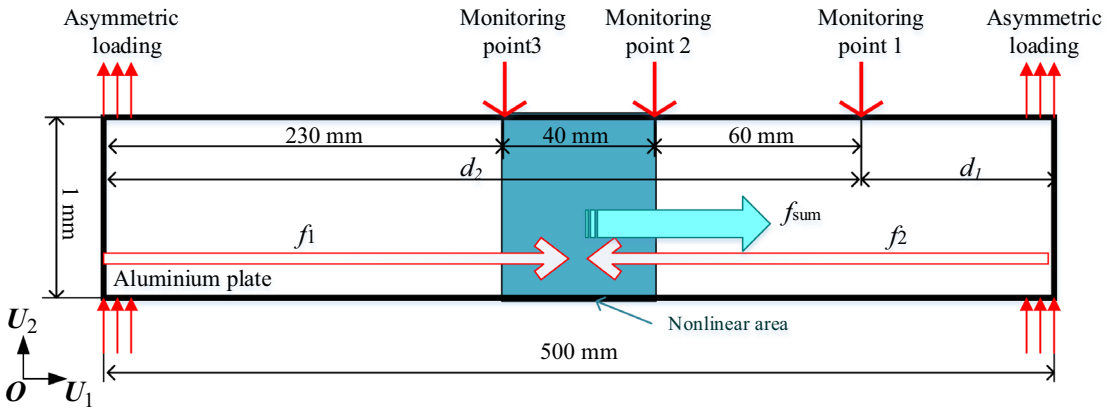

Figure 3 Schematic diagram of finite element model

Table 1 Properties of nonlinear elastic materials

Density	Second order elastic constant		Third order elastic constant		
ρ(kg/m^3)	E(GPa)	υ	l (GPa)	m(GPa)	n(GPa)
2700	70	0.33	− 250	− 333	− 350

that the sum-frequency S0 wave propagates in the same direction as one of the incident waves.

3 Finite Element Simulation

The relationship between the third-order elastic constants of materials and their stresses has been clarified in numerous studies [34, 35]. To validate the Lamb wave mixing technique for local stress measurements, numerical simulations of Lamb wave mixing were performed. In the simulation model, the local stresses of the structure were simulated by varying the local third-order elastic constants.

3.1 Finite Element Model

A two-dimensional finite element model of thin plates with local material anomalies was constructed using the commercial finite element software ABAQUS, as shown in Figure 3.

An aluminum sample with cross-section of 500 mm × 1 mm is modeled. To simulate localized stress concentrations, the material properties of a localized area with 40 mm ×1 mm at the center of the model were set to nonlinear, and the material properties of the rest of the model were set to linear elasticity. The nonlinear elastic parameters are listed in Table 1, and the elastic parameters associated with the linear elasticity were consistent with those of the nonlinear elasticity. Two excitation signals with different frequencies (f_1 and f_2) were applied

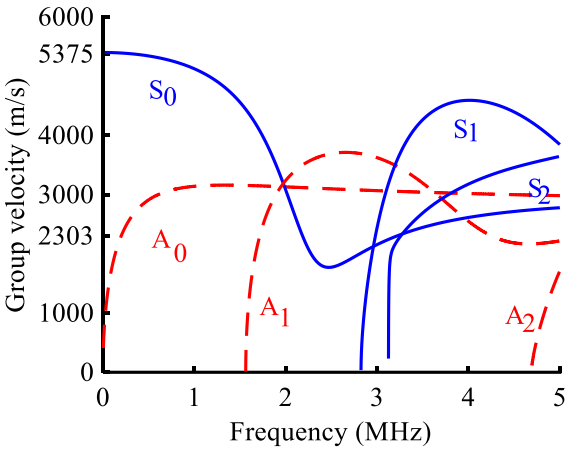

Figure 4 Group velocity dispersion curve in 1-mm-thick aluminum plate

to each side of the model in an antisymmetric loading manner. Three monitoring points located at the upper surface, i.e., 330, 270, and 230 mm away from the left end, were used to receive the displacement in the U2 (off-plane) direction.

In addition to satisfying the resonant conditions, another necessary condition for generating wave-mixing effect is that the two incident waves must coincide at the nonlinear source. This implies that two incident waves must reach the nonlinear region simultaneously. Based on the difference in the group velocity of the two excitation signals (as shown in Figure 4), the time delay of the two excitations was determined to be 1.4×10^{-5} and 0 s. Table 2 lists the primary parameters of the two excitation signals. The excitation signal in the simulations was a sinusoidal signal modulated by a Hanning window.

For comparison, a finite element simulation of the complete linear elasticity model was performed under the same conditions. The finite element model showed

Table 2 Parameters of excitation signal

	Mode type	Frequency (MHz)	Amplitude (mm)	Delay (s)	Cycle
f_1	A0	1.26	0.05	1.45×10^{-5}	40
f_2	A0	0.32	0.05	0	10

no local material anomalies. These two models are hereinafter referred to as the nonlinear and linear models, respectively.

3.2 Simulation Results and Discussion

Figure 5 shows the waveforms and spectra received by monitoring point 1 in the linear and nonlinear models. The signals received from the two models were different; however, it was difficult to determine the mode and frequency of each echo from waveform. Two new frequency components appeared in the spectrum of the signal received by the nonlinear model: the second harmonics (0.64 MHz) and sum-frequency component (1.58 MHz).

Figure 6 shows the time–frequency distribution of the two signals processed by the continuous wavelet transform. The time–frequency results show two distinct peaks in the time–frequency distribution of the signal obtained from the linear model, which corresponded to the two A0 waves at the fundamental frequency.

The signal obtained from the nonlinear model contained five separated echoes in the waveform; however, the time–frequency distribution of the second and third echoes contained two frequency components, which resulted in seven distinct peaks in the time–frequency distribution.

Using the travel time, central frequency, and possible propagation paths of each echo (as shown in Figures 5 and 6), their velocities can be calculated; consequently, the mode of each echo can be determined. Table 3 summarizes the analysis process and the results for each echo. Echo "1" is the first arriving packet, and it is the second harmonics of the S0 wave (0.64 MHz) generated by the excitation signal at $f_2 = 0.32$ MHz. Echo "2" includes two components, i.e., the fundamental component (0.32 MHz) and the second harmonics (0.64 MHz) of the A0 wave generated by the excitation signal at

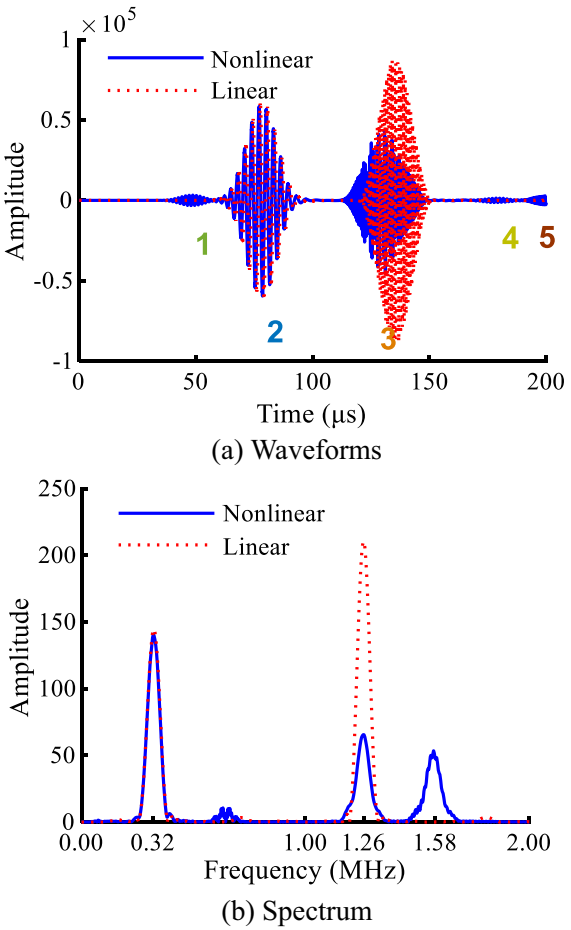

Figure 5 Waveform and spectrum obtained from two models at point 1

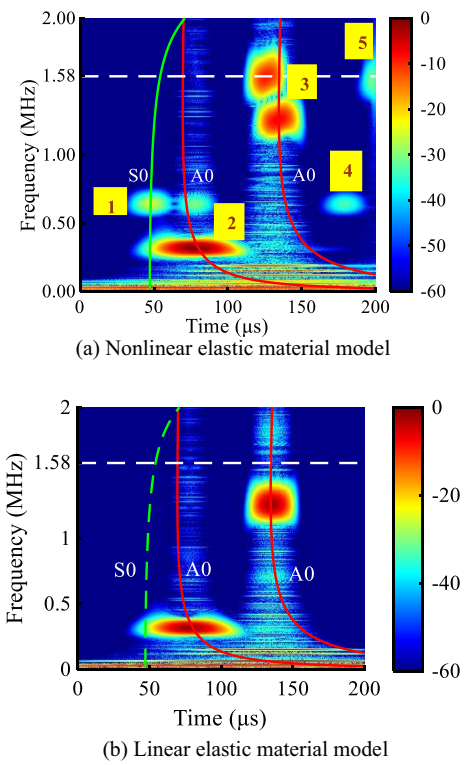

Figure 6 Time–frequency distributions of signals obtained from two models

Table 3 Analysis process and results for each echo

Echo number	1	2		3		4	5
Propagation path	d_1	d_1		d_2		d_2+d_2	d_1+d_1
Time of arrival(μs)	t_1	t_2		t_3	t_{sum}	t_4	t_5
	48.65	78.08		134.4	126.7	178.8	199.6
Travel time	t_1	t_2		t_3	–	t_1–t_4	t_5–t_{sum}
Mode(MHz)	S0 0.64	A0 0.32	A0 0.64	A0 1.26	S0 1.58	S0 0.64	S0 1.58
Calculating velocity(m/s)	5139	2128	–	3163	–	5071	4664
Theoretical velocity(m/s)	5300	2646	–	3159	–	5300	4406

$f_2 = 0.32$ MHz. Notably, the geometric nonlinearity enabled in the simulations allowed the generation of the second harmonics in the linear material region. Echo "3" includes two components, i.e., the fundamental component (1.26 MHz) of the A0 wave generated by the excitation signal at $f_1 = 1.26$ MHz, and the sum-frequency component (1.58 MHz) of the S0 wave generated by the interaction of two incidents. Echo "4" is the echo reflected by echo "1" at the left boundary. Echo "5" is the echo reflected by the sum-frequency (1.58 MHz) S0 wave at the right boundary.

To further illustrate that the sum-frequency component was generated by the interaction of two incident A0 waves, numerical simulations were performed on the nonlinear model under the individual and synchronous excitation of two incident waves.

Figures 7 and 8 present the waveforms and spectra of the simulation signals received at monitoring points 2 and 3, respectively, including the signals obtained under synchronous excitation, sum of signals obtained under individual excitations, and difference between signals under individual and synchronous excitations.

As indicate by the signals detected at monitoring point 2 in Figure 7, the signals under individual and synchronous excitations differed significantly.

Specifically, a distinct echo was observed in the waveform of the differential signal with a center frequency exactly at a sum frequency of 1.58 MHz. However, no sum-frequency component was observed in the spectrum of the signals under individual excitations. Therefore, the sum-frequency component was generated by the interaction of two incident A0 waves under synchronous excitations, and no sum-frequency component was generated under individual excitations of the two A0 waves.

A similar analysis can be performed for the signals received at monitoring point 3, as shown in Figure 8.

Similarly, a discernible echo was observed in the differential signal detected at monitoring point 3. However, the echo at monitoring point 3 differed significantly from that at monitoring point 2, i.e., it featured a smaller amplitude, an earlier arrival time, and a center frequency

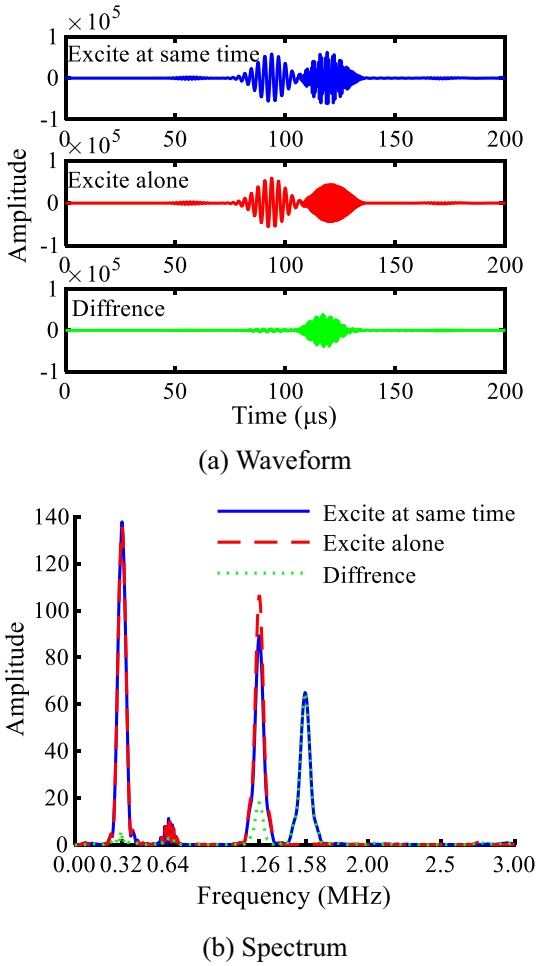

Figure 7 Results received at point 2 under different excitations

of 0.64 MHz. The echo was identified as the second-harmonic component at 0.64 MHz, which was generated under both individual and synchronous excitations; furthermore, the second-harmonic components obtained from the two monitoring points were similar. Notably, no discernible sum-frequency component was observed in the signals detected at monitoring point 3. Therefore, it can be inferred that the sum-frequency wave was

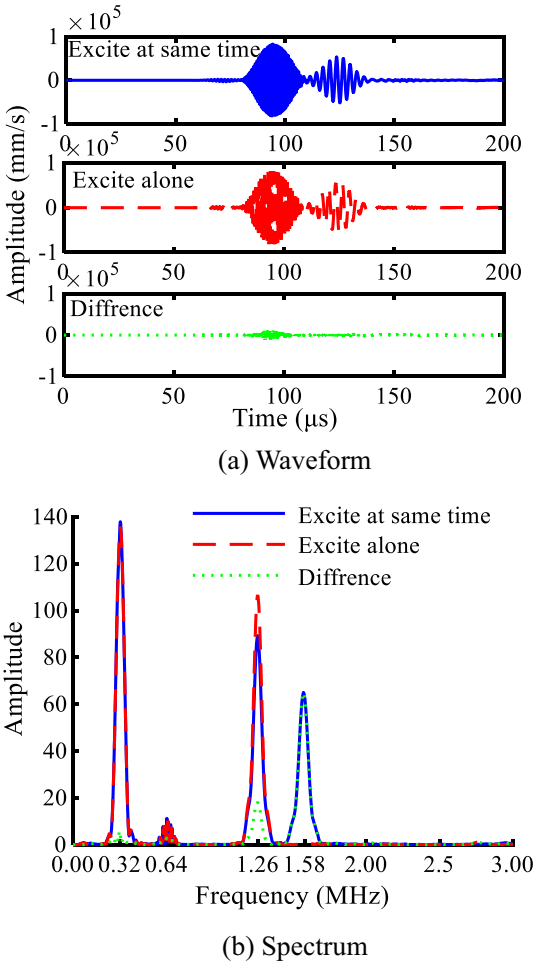

Figure 8 Results received at point 3 under different excitations

generated at the intersection of two incident A0 waves and propagated to the right. This is consistent with the propagation direction determined based on the theoretical resonance conditions.

To show the nonlinear interaction of two incident A0 waves more clearly, the displacement distribution of the points on the horizontal plane in the middle of the plate at typical moments is shown in Figure 9. The displacements in the U_1 and U_2 directions are plotted in red and blue, respectively. The wave propagation process can be observed clearly. The two incident A0 waves propagated in opposite directions, and a rightward propagating S0 wave was generated at the intersection.

4 Experiments for Stress Distribution Measurement

Collinear Lamb wave mixing experiments were conducted to investigate the effectiveness of the mixing technique for measuring the residual stress distribution in metal plates.

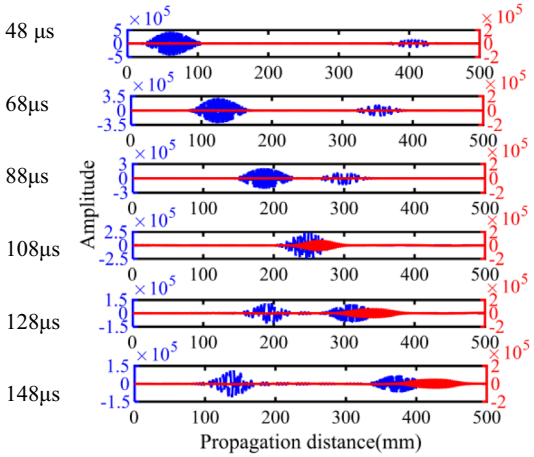

Figure 9 Images of U_2 (blue) and U_1 (red) displacement components along the line

4.1 Finite Element Model

Figure 10 shows a schematic illustration of the collinear wave-mixing measurement system. The SNAP RAM-5000 is the core component of the nonlinear measurement system. Two high-voltage signals from the output of "RF burst" channels were applied to the two piezoelectric transducers (A and B).

The central frequencies of the two transmitters were 0.304 and 0.77 MHz. Lamb waves were received by a piezoelectric transducer located at the midpoint of the connection between the two transmitters. The center frequency of the receiver was 1 MHz. The frequency responses of the three transducers above are shown in Figure 11.

Considering the frequency response of the transmitters and receiver (shown in Figure 11(a)), the center frequency f_1 of the excitation signal applied to transmitter A was 0.304 MHz. To obtain a strong mixing-frequency nonlinear response, the effect of the driving frequency f_2 on the amplitude of the sum-frequency component was investigated via frequency-sweep experiments. The driving frequency f_2 applied to transmitter B was varied from 0.2 to 2 MHz at intervals of 0.05 MHz. Figure 11(b) shows the frequency dependence of the sum-frequency component when f_1 was 0.304 MHz. The amplitudes of the sum-frequency component were particularly sensitive to the driving frequency, and four local resonant points were observed. Specifically, three resonant points (0.304, 0.636, and 0.95 Hz) corresponded to the fundamental and harmonic components of f_1. At these three resonance points, the sum-frequency components were the higher harmonics of the primary waves that were susceptible to system nonlinearity. To avoid the effect of nonlinearity on harmonic generation, the center frequency f_2 of

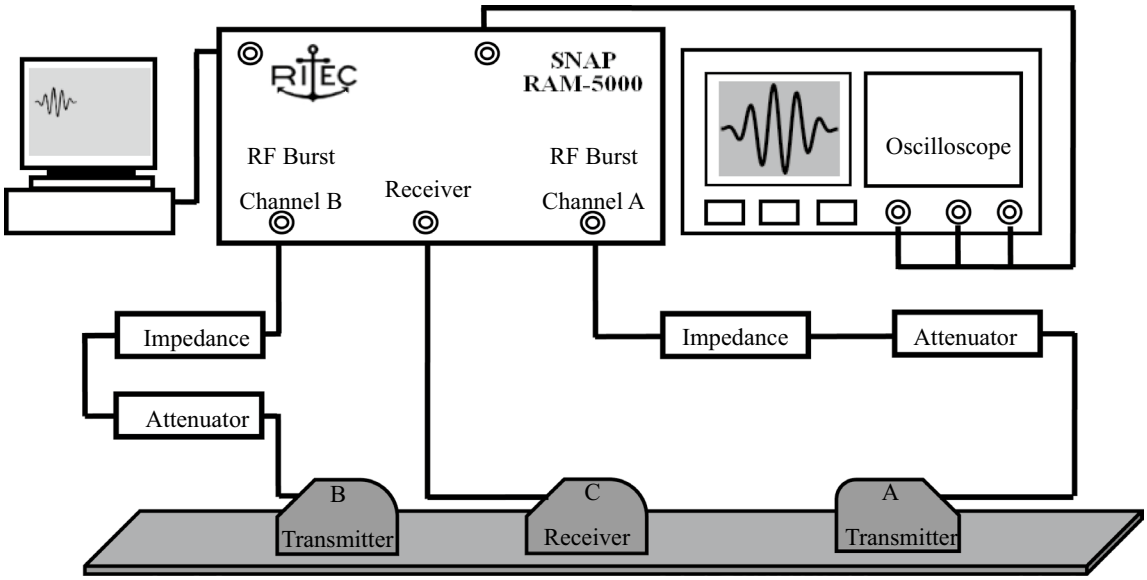

Figure 10 Schematic diagram of experimental system

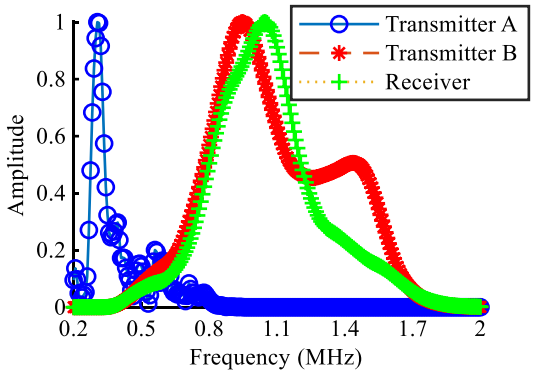

(a) Frequency response of transducers

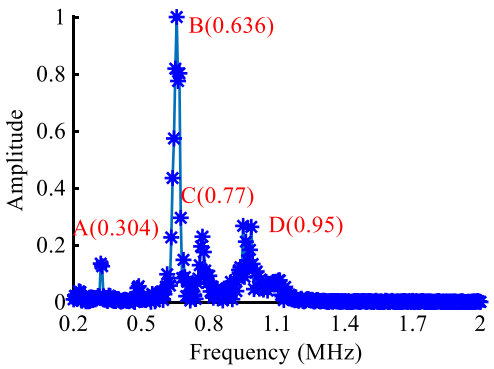

(b) Frequency dependence of sum-frequency

Figure 11 Sweep curve of frequency response

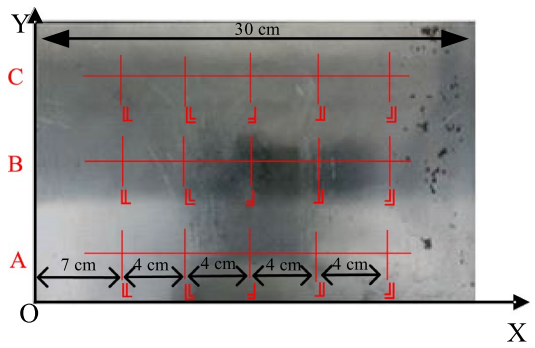

(a) Embryo block specimen

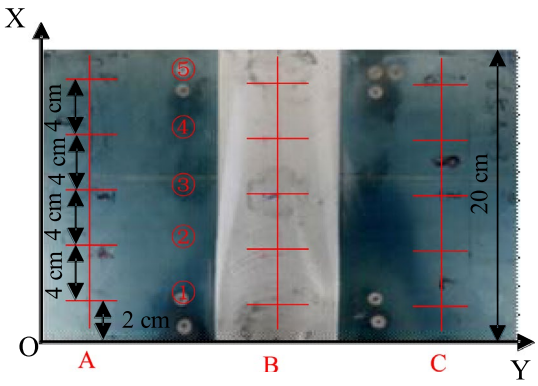

(b) Milling specimen

Figure 12 Specimens

Table 4 X-ray results of residual stress distribution in specimens

Position	Embryo block specimen			Milling specimen		
(MPa)	A	B	C	A	B	C
1	− 15	− 46.5	− 64.4	− 94.4	− 158.2	− 61.7
2	− 59.3	− 143	− 40.9	− 6.9	− 203.3	41.8
3	− 135.1	− 85	− 35.6	9.8	− 322.8	− 3.8
4	− 100.8	− 27.1	− 75.5	35.2	− 302.7	43.9
5	− 84.4	3.3	− 106.2	− 13.7	− 610	− 26.6

the excitation signal applied to transmitter B was set to 0.77 MHz. Table 5 lists the specific parameters of the two excitation signals.

The experimental measurements were conducted on two 65 Mn steel sheets with dimensions of 300 mm × 200 mm × 3 mm, as shown in Figure 12.

Both specimens were sampled from an industrial component with a local residual stress. A rectangular area of 200 mm × 75 mm in the middle of specimen 2# was partially machined, as shown in Figure 12(b). Residual stresses were measured using X-rays at 15 typical positions on three straight lines in the specimen; the measured residual stresses are listed in Table 4.

Figure 13 presents the experimental scheme for the stress measurement via collinear Lamb wave mixing. In the experiment, one transmitter was placed at each of the two ends of three straight lines, i.e., A–A, B–B, and C–C, and the receiver was placed in the center of the connection between the two transmitters. During the stress measurement, the positions of the transmitters and receiver were fixed. Different delays were set for the two transmitters such that the intersection position of two Lamb waves can be controlled. The receiver was used to receive the generated Lamb waves at the sum-frequency. Thus, the spatial sweep of the ultrasonic beam intersection can be regarded as a measurement of nonlinearity at different spatial locations in the metal plate. If the attenuation is disregarded, then the sum-frequency component in the measured signal will be related to the stress level at the intersection point.

4.2 Experimental Results and Discussion

Compared with the linear response, the nonlinear response was relatively weak. Therefore, collinear Lamb wave mixing experiments were conducted to investigate the extraction of mixed-frequency nonlinear components from the detected signals. The receiver picked up the signals when the two transmitters were excited simultaneously and respectively. Specifically, the superposition of the received signals obtained by applying the excitations respectively is known as the "sum of signals received through separate excitations." The difference between the "sum of signals received through separate excitations" and the "sum of signals received through simultaneous excitations" was used to analyze the nonlinear effects.

Figure 14 shows the typical signals obtained from the collinear Lamb wave mixing experiments. The waveforms of the sum of signals received through separate excitations were similar to those received through simultaneous excitations, i.e., they contained the direct wave and reflected echo of the A0 mode at 50 and 150 μs. However, the waveform of the difference signal contained only direct waves. The corresponding spectrum presented in Figure 14(b) shows that each signal contained multiple frequency components. In particular, no mixed-frequency component was observed in the spectrum of the sum of signals received through separate excitations.

Under the same experimental setup, collinear Lamb wave mixing experiments were conducted by reversing the polarities of the two excitations, i.e., the phases of the two excitations were (0°, 0°), (0°, 180°), (180°, 0°), and (180°, 180°). The superposition of the detection signals obtained at four different polarity combinations is known as the "polarity reversal signal."

Figure 15 shows a comparison of the polarity reversal results and the difference signals. In the time domain, the amplitude of the difference signal exceeded that of the polarity reversal signal.

Furthermore, the spectrum presented in Figure 15(b) shows that the difference signal contained more components than the polarity reversal signal. Twelve components were observed in the spectrum of the difference signal: 0.15, 0.304, 0.46, 0.608, 0.77, 0.92, 1.074, 1.22, 1.46, 1.53, 1.716, and 1.824 MHz. However, four components were observed in the spectrum of the polarity

Table 5 Parameters of excitation signal

	Mode type	Frequency(MHz)	Cycle	Signal feature
f_1	A0	1.26	40	Sinusoidal signal modulated by Hanning window
f_2	A0	0.32	10	

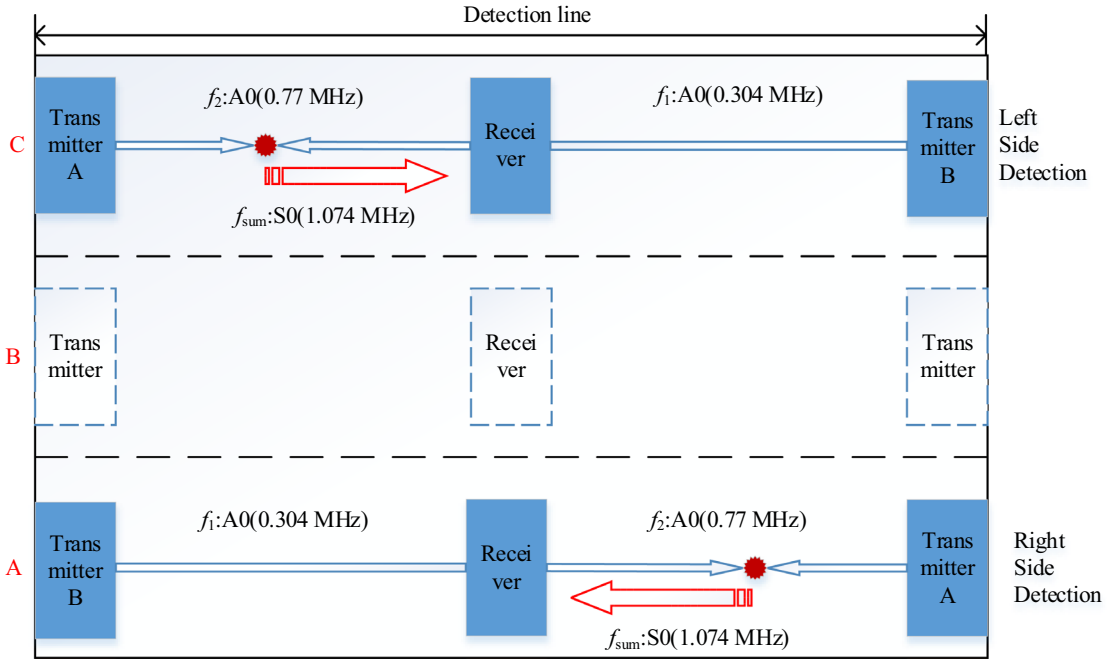

Figure 13 Experimental scheme for stress distribution measurement

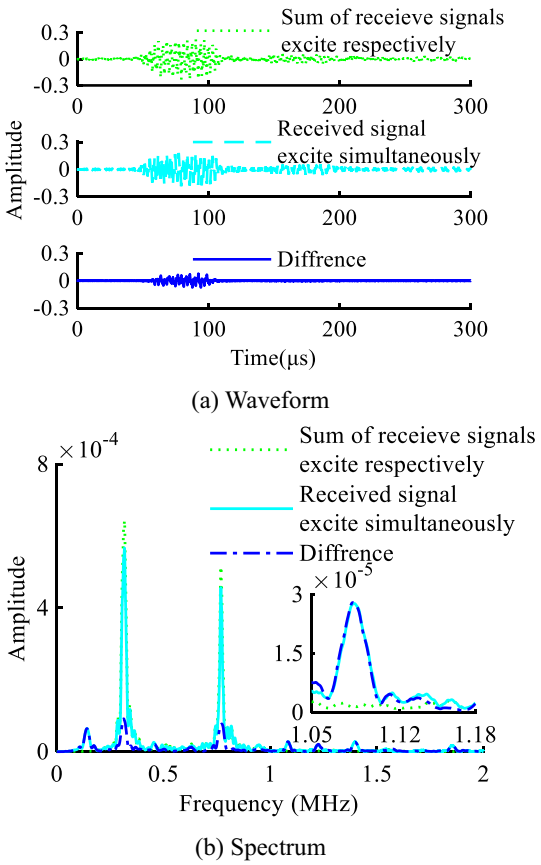

Figure 14 Typical signals obtained from collinear Lamb wave mixing experiments

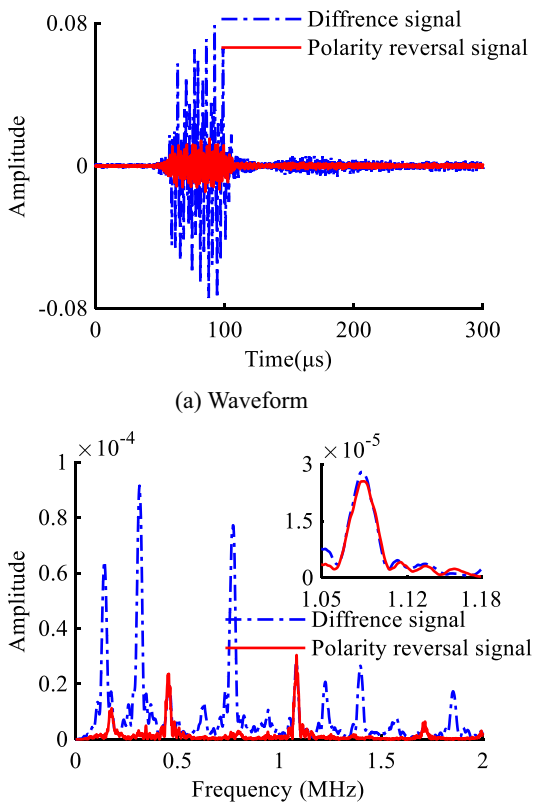

Figure 15 Comparison of nonlinear component extraction

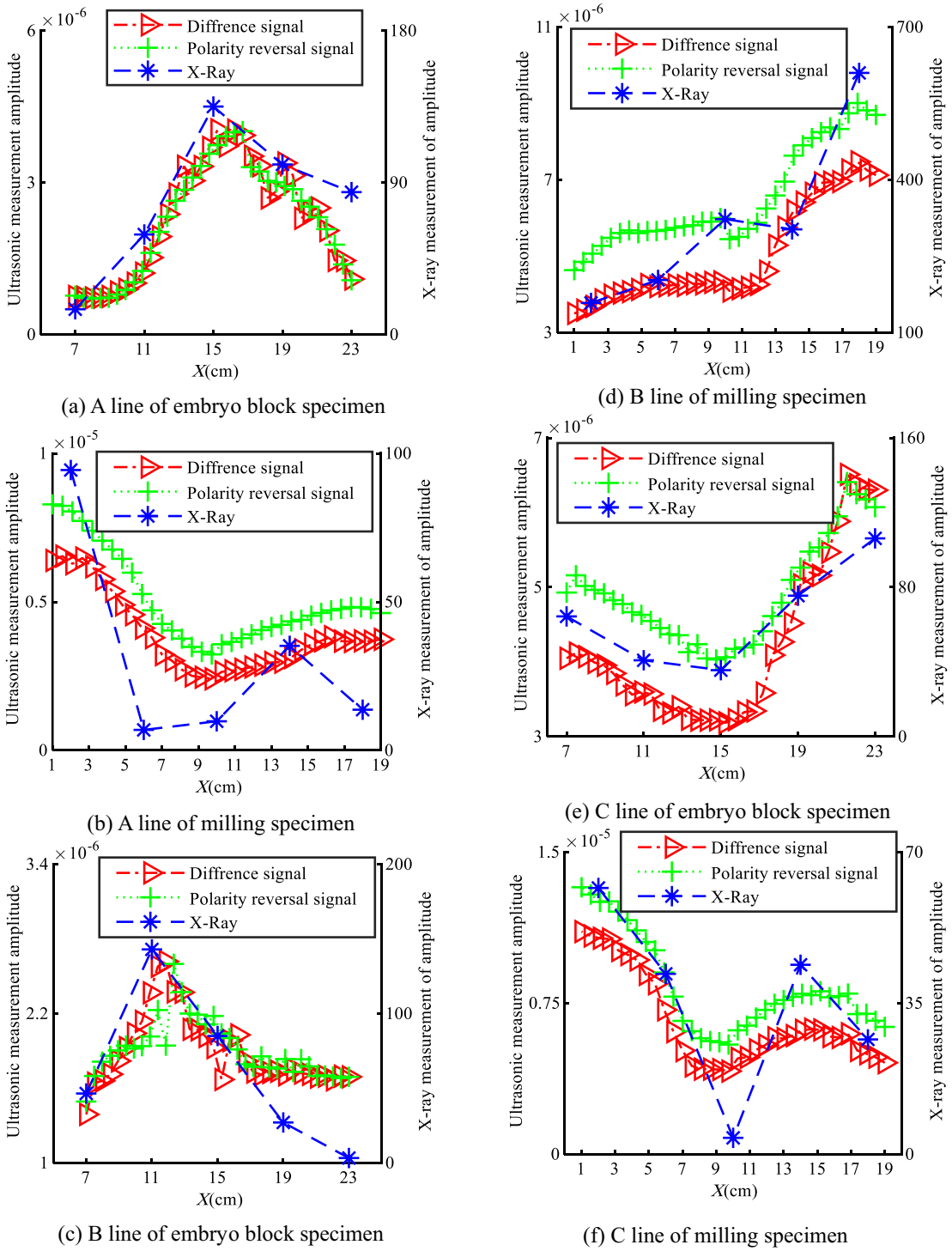

Figure 16 Results of stress measurement

reversal signal: 0.165, 0.46, 1.074, and 1.716 MHz. The generation of each component can be analyzed specifically based on the center frequency of the two excitation signals (f_1 = 0.304 MHz and f_2 = 0.77 MHz). In detail, the components at 0.15, 0.304 0.608, 0.77, 0.92, 1.22, 1.46, 1.53, and 1.716 were regarded as the subharmonic or higher harmonic response of the two excitations. The components at 1.074 and 0.46 MHz were regarded as

the sum-frequency and difference-frequency responses of the two excitations, respectively. The component at 1.716 MHz was regarded as the sum-frequency response generated by the subharmonic of f_1 (0.152 MHz) and second harmonics of f_2 (1.54 MHz). The component at 0.165 MHz was regarded as the difference-frequency response generated by the fundamental f_2 (0.77 MHz) and second harmonics of f_1 (0.608 MHz). Multiple harmonic components were observed in the difference signal; however, no harmonic components were observed in the polarity reversal signal. To avoid the effects of harmonics generated by system nonlinearity, the polarity reversal signals should be used to extract the mixed-frequency nonlinear component. In this study, the sum-frequency component at 1.074 MHz was extracted from both the difference and polarity reversal signals; subsequently, it was used to characterize the residential stress.

Figure 16 presents the amplitude of the sum-frequency component (measured via collinear Lamb wave mixing experiments) and stress (measured by X-rays) at different spatial locations. In general, the spatial distribution of the amplitudes of the sum frequency components measured via the two methods was similar to that of the residual stresses measured using X-rays. Therefore, the proposed amplitude of the sum-frequency component can be used to evaluate the residential stress in a metal structure. However, the amplitude of the sum-frequency component fluctuated significantly in the local spatial range (as shown in Figure 16(c)) and deviated considerably from the stress distribution.

This is attributable to the average effect and insufficient spatial resolution due to the probe size, delay errors, attenuation of ultrasonic waves, etc. In future investigations, immersion-focusing probes will be used to improve the spatial resolution and repeatability of the measurements.

5 Conclusions

In this study, collinear Lamb wave mixing was adopted to measure the residual stress in metal plates.

(1) Based on theoretical analysis, the resonant conditions required for two Lamb waves to generate a mixing frequency wave were obtained. Finite element simulations were performed to investigate the nonlinear interactions between the two Lamb waves. Results showed that two incident A0 waves interacted in regions of material nonlinearity and generated an S0 wave at the sum-frequency. Moreover, the generated S0 wave propagated to the right, which was consistent with the propagation direction determined based on the theoretical resonance conditions.
(2) The excitation frequencies for the Lamb wave mixing experiments were determined by considering both the theoretical resonance conditions and the experimental amplitude-frequency dependence of the sum-frequency component.
(3) Residual stress measurement experiments were conducted on steel plate specimens using the collinear Lamb wave mixing technique. By setting different delays for the two transmitters, the generated sum-frequency component at different spatial locations was measured. The experimental results showed that the spatial distribution of the amplitude of the sum-frequency component agreed well with the spatial distribution of the residual stress measured using X-rays.

Therefore, the proposed collinear Lamb wave mixing method is effective for measuring the distribution of residual stress in metal plates.

Acknowledgements
Supported by National Natural Science Foundation of China (Grant Nos. 11972053, 12274012).

Author Contributions
JJ, LL were in charge of the whole trial; JJ and LL wrote the manuscript; QC and XG assisted with experiments; QC assisted with FE modeling; CH and BW assisted with framework design of manuscript. All authors read and approved the final manuscript.

Authors' Information
Jingpin Jiao, born in 1973, is currently a professor at *Faculty of Materials and Manufacturing, Beijing University of Technology, China*. Her research interests include nondestructive testing, experimental mechanics, and signal process.
Li Li, born in 1992, is currently a PhD candidate at *Faculty of Materials and Manufacturing, Beijing University of Technology, China*. He received his Bachelor degree from *Anhui Jianzhu University, China*, in 2013.
Xiang Gao, born in 1991, is currently a lecture at *Faculty of Materials and Manufacturing, Beijing University of Technology, China*. His research interests include nondestructive testing, ultrasonic imaging.
Quan Cheng, born in 1994. She received master degree from *Beijing University of Technology, China*, in 2019.
Cunfu He, born in 1958, is currently a professor at *Faculty of Materials and Manufacturing, Beijing University of Technology, China*. His research interests include nondestructive testing, experimental mechanics.
Bin Wu, born in 1962, is currently a professor at *Faculty of Materials and Manufacturing, Beijing University of Technology, China*. His research interests include nondestructive testing, experimental mechanics.

Data availability statement
The data that support the findings of this study are available on request from the corresponding author. The data are not publicly available due to privacy.

Competing interests
The authors declare no competing financial interests.

Received: 1 February 2021 Revised: 18 May 2022 Accepted: 2 January 2023
Published online: 31 January 2023

References

[1] M M Shokrieh. Residual stresses in composite materials. *Residual Stresses in Composite Materials*, 2014: 350-373.
[2] R F Charles, W Keith. An introduction to structural health monitoring. *Philosophical Transactions of the Royal Society A: Mathematical, Physical and Engineering Sciences*, 2007, 365(1851): 303-315.
[3] R Bullough, V R Green, B Tomkins, et al. A review of methods and applications of reliability analysis for structural integrity assessment of UK nuclear plant. *International Journal of Pressure Vessels and Piping*, 1999, 76(13): 909-919.
[4] Youtsos, Anastasius. Residual stress and its effects on fatigue and fracture. *Springer Netherlands*, 2006.
[5] X F Huang, Z W Liu, H M Xie. Recent progress in residual stress measurement techniques. *Acta Mechanica Solida Sinica*, 2013, 26(6): 570-583.
[6] N S Rossini, M Dassisti, K Y Benyounis, et al. Methods of measuring residual stresses in components. *Materials & Design*, 2012, 35(119): 572-588.
[7] X Zhu, F Scalea, M Fateh. Thermal stress measurement in continuous welded rails using the hole-drilling method. *Experimental Mechanics*, 2017, 57(1): 165-178.
[8] G S Schajer. Relaxation methods for measuring residual stresses: techniques and opportunities. *Experimental Mechanics*, 2010, 50(8): 1117-1127.
[9] C G Xu, H X Li, J F Wang, et al. Ultrasonic shear and longitudinal wave testing method of residual stress. *Acta Acustica*, 2017, 42(2): 195-204. (in Chinese)
[10] A J Allen, M T Hutchings, C G Windsor, et al. Neutron diffraction methods for the study of residual stress fields. *Advances In Physics*, 1985, 34(4): 445-473.
[11] C H Ma, J H Huang, H Chen. Residual stress measurement in textured thin film by grazing-incidence X-ray diffraction. *Thin Solid Films*, 2002, 418(2): 73-78.
[12] T C Chu, W F Ranson, M A Sutton, et al. Applications of digital-image correlation techniques to experimental mechanics. *Experimental Mechanics*,1985, 25(3): 232-244.
[13] L Mierczak, D C Jiles, G Fantoni. A new method for evaluation of mechanical stress using the reciprocal amplitude of magnetic Barkhausen noise. *IEEE Transactions on Magnetics*, 2011, 47(2): 459-465.
[14] H J Lim, H Sohn. Online stress monitoring technique based on Lamb wave measurements and a convolutional neural network under static and dynamic loadings. *Experimental Mechanics*, 2020, 60(1): 171-179.
[15] P R L Alves, J S C Filho, M G Farinhas. A new approach to determine tensile stress states from the parameters of longitudinal waves. *Applied Mathematical Modelling*, 2020, 83(1): 189-201.
[16] H Kim, T Kim, D Morrow, et al. Stress measurement of a pressurized vessel using ultrasonic subsurface longitudinal wave with 1-3 composite transducers. *IEEE Transactions on Ultrasonics, Ferroelectrics, and Frequency Control*, 2020, 67(1): 158-165.
[17] W Wang, C Xu, Y Zhang, et al. An improved ultrasonic method for plane stress measurement using critically refracted longitudinal waves. *NDT&E International*, 2018, 99(1): 117-122.
[18] S Chaki, W Ke, H Demouveau. Numerical and experimental analysis of the critically refracted longitudinal beam. *Ultrasonics*, 2013, 53(1): 65-69.
[19] Y Chen, C S Man , K Tanuma , et al. Monitoring near-surface depth profile of residual stress in weakly anisotropic media by Rayleigh-wave dispersion. *Wave Motion*, 2018, 77(1): 119-138.
[20] M Mohammad, J J Fesharaki. Termination of acoustoelastic acoustoplastic constants to measure stress in elastic/plastic limits by using LCR wave. *NDT &E International*, 2019, 104(1): 69-76.
[21] W Wang, Y M Zhang , Y F Zhou, et al. Plane stress measurement of orthotropic materials using critically refracted longitudinal waves. *Ultrasonics*, 2019, 94(1): 430-437.
[22] M X Deng. Cumulative second-harmonic generation accompanying nonlinear shear horizontal mode propagation in a solid plate. *Journal of Applied Physics*, 1998, 84(7): 3500-3505.
[23] X Y Ding, Y X Zhao, M X Deng, et al. One-way Lamb mixing method in thin plates with randomly distributed micro-cracks. *International Journal of Mechanical Sciences*, 2020, 171(1): 105371.
[24] H Chen, G Gao, N Hu, et al. Modeling and simulation of frequency mixing response of two counter-propagating Lamb waves in a two-layered plate. *Ultrasonics*, 2020, 104(1): 106109.
[25] A N Li , B Yuan, Y Z Wang, et al. Diode behavior and nonreciprocal transmission in nonlinear elastic wave metamaterial. *Mechanics of Materials*, 2019, 133(1): 85-101.
[26] G J Kim, S J Park, H G Kwak. Application of nonlinear ultrasonic method for monitoring of stress state in concrete. *Journal of the Korean Society for Nondestructive Testing*, 2016, 36(2): 121-129.
[27] K Y Jhang. Nonlinear ultrasonic techniques for nondestructive assessment of micro damage in material: A review. *International Journal of Precision Engineering & Manufacturing*, 2009, 10(1): 123-135.
[28] H Hu, Z Zou, Y Jiang, et al. Finite element simulation and experimental study of residual stress testing using nonlinear ultrasonic surface wave technique. *Applied Acoustics*, 2019, 154 (1): 11-17.
[29] H J Yan, F B Liu, Q X Pan. Nonlinear ultrasonic properties of stress in 2024 Aluminum. *Advanced Materials Research*, 2017, 1142(1): 371-377.
[30] M H Liu, J Y Kim, L Jacobs, et al. Experimental study of nonlinear Rayleigh wave propagation in shot-peened aluminum plates- feasibility of measuring residual stress. *NDT&E International*, 2011, 44(1): 67-74.
[31] H L Mao, Y H Zhang, H Y Mao, et al. Stress evaluation of metallic material under steady state based on nonlinear critically refracted longitudinal wave. *Results in Physics*, 2018, 9(1): 665-672.
[32] J P Jiao, X J Meng, C F He, et al. Nonlinear Lamb wave-mixing technique for micro-crack detection in plates. *NDT&E International*, 2017, 85(1): 63-71 。
[33] A J Croxford, P D Wilcox, B W Drinkwater, et al. The use of non-collinear mixing for nonlinear ultrasonic detection of plasticity and fatigue. *The Journal of the Acoustical Society of America*, 2009, 126(5): 117-122.
[34] M Liu, J Y Kim, J M Qu, et al. Measuring residual stress using nonlinear ultrasound. *AIP Conference Proceedings*, 2010, 1211(1): 1365-1372.
[35] V K Chillara, C J Lissenden. Nonlinear guided waves in plates: a numerical perspective. Ultrasonics, 2014,54(6): 1553–1558.